Chinese Journal of
POLYMER SCIENCE

RESEARCH ARTICLE

https://doi.org/10.1007/s10118-023-3028-x
Chinese J. Polym. Sci. **2024**, *42*, 256–266

Highly Improved Creep Resistance in Polypropylene Through Thermally Reduced Graphene Oxide and Its Creep Lifetime Prediction

Can-Can Zhang, Jun-Long Yang*, Ya-Jiang Huang, and Guang-Xian Li

College of Polymer Science and Engineering, State Key Laboratory of Polymer Materials Engineering of China, Sichuan University, Chengdu 610065, China

Abstract Polypropylene (PP) exhibits suboptimal creep resistance due to the presence of methyl groups on its main chain, leading to irregular chain segment distribution, diminished inter-chain interaction, and crystallinity. This structural feature causes chain slippage in PP under stress, significantly constraining its service lifetime. In this study, thermally reduced graphene oxide (TrGO) nanosheets were incorporated into the PP matrix, yielding a nanocomposite with exceptional creep resistance performance. Results demonstrated that at a stress of 25 MPa, a 2.0 wt% TrGO content could enhance the creep failure lifetime of PP by 21.5 times compared to neat PP. Rheology, transmission electron microscopy (TEM), and scanning electron microscopy (SEM) characterization techniques were employed to analyze the mechanism of TrGO's influence on PP's creep behavior. It was observed that when TrGO content exceeded 1.0 wt%, an effective particle network structure formed within the PP matrix. This homogeneously dispersed TrGO-formed particle network structure restricted the migration and rearrangement of PP molecular chains, enabling prolonged stress resistance without structural failure. By combining the time-strain superposition method with the critical failure strain as a criterion, generalized creep compliance curves for PP and its composites were established, facilitating the prediction of material creep failure lifetimes, with a strong agreement between experimental and predicted lifetime values. This research proposes a novel strategy aimed at developing polypropylene materials and products with enhanced long-term stability and durability, thus extending service life, reducing failure risk, and broadening their potential across various application domains.

Keywords Thermally reduced graphene oxide; Polypropylene; Creep failure and lifetime prediction

Citation: Zhang, C. C.; Yang, J. L.; Huang, Y. J.; Li, G. X. Highly improved creep resistance in polypropylene through thermally reduced graphene oxide and its creep lifetime prediction. *Chinese J. Polym. Sci.* **2024**, *42*, 256–266.

INTRODUCTION

Polypropylene (PP), as one of the five primary general plastics, is extensively used in various applications, including packaging, automotive components, construction materials, electronic devices, and textiles as structural components and base materials.[1,2] The mechanical stability of PP is of paramount importance due to its structural function in most applications. Factors that often determine its service lifetime include the material's creep and fatigue resistance (anti-fracture performance) under cyclic or constant loading conditions. However, PP, a thermoplastic non-polar material, exhibits relatively low creep resistance and suboptimal dimensional stability. This is attributed to the presence of methyl groups in the main chain, which diminish the regularity of its molecular chains, resulting in weaker intermolecular forces and reduced crystallinity.[3] Consequently, addressing the issue of low creep resistance is essential for not only broadening the range of applications of PP, but also for extending the service lifetime of PP products. As such, research into enhancing the creep resistance of polypropylene is of great significance and has practical implications in various industries.

Graphene, a novel carbon material, features a unique two-dimensional honeycomb lattice structure composed of closely packed single-layer carbon atoms.[4] Owing to its outstanding mechanical, thermal, and electrical properties, graphene has emerged as a focal point of research in various fields such as new nanomaterials, electronics, and electrical appliances in recent years.[5–8] The modulus of single-layer graphene can reach an impressive 1 TPa.[9] Studies on PP/graphene composites reveal that incorporating even a small amount of graphene significantly enhances mechanical properties, including tensile strength, flexural strength, and Young's modulus.[10–12] Zandiatashbar *et al*. showed that,[13] under elevated temperatures and stress, the creep behavior of epoxy resins can be substantially inhibited with 0.1 wt% graphene content, outperforming single-walled carbon nanotubes (SWNTs) and multi-walled carbon nanotubes (MWNTs). Tang *et al*. investigated the impact of carbon materials with three distinct dimensional structures on the creep behavior of polystyrene (PS).[14,15] They found that, compared to three-dimensional carbon black (CB) and one-dimensional carbon nanotubes (CNT), graphene's two-dimensional layered structure more effectively restricts the mobility of polymer molecular chains when subjected to external forces. This constraint limits

* Corresponding author, E-mail: email: yangjl@scu.edu.cn
Received May 18, 2023; Accepted July 11, 2023; Published online July 20, 2023

molecular chain migration and rearrangement, thereby considerably suppressing the creep behavior of PS. By incorporating hydrothermally reduced graphene oxide (RGO) into the PP matrix, the creep resistance and recoverability of PP/RGO composites can be improved at high temperatures.[16] These findings demonstrated the vast potential of graphene in enhancing the creep resistance of polymer materials, opening up new avenues for the development of advanced composites with superior mechanical performance, durability and wider application possibilities across a range of industries.

Furthermore, the accelerated creep lifetime prediction for polymer materials holds significant implications, which is crucial for ensuring product safety during actual use, mitigating the risks associated with material creep-induced damage or failure. It has been observed that the transition from secondary to tertiary creep in PP consistently occurs at a constant strain (critical failure strain, ε_{cr}) across various stress levels.[17,18] In our previous research, we utilized a combined time-strain superposition method[19–21] to characterize and predict the creep behavior and failure lifetime of PP/clay nanocomposites.[3] The results demonstrated that employing the critical failure strain as a criterion enables the extraction of the lifetime description equation for composite materials through accelerated creep tests under high-stress conditions. This approach facilitates the prediction of creep failure lifetimes under low-stress conditions, offering a convenient and efficient method for rapidly predicting the nonlinear creep failure lifetimes of polymer materials.

In this work, we first prepared graphene using a thermal reduction method.[22] Compared to alternative preparation techniques, thermally reduced graphene oxide (TrGO) has gained extensive acceptance due to its cost-effective, rapid processing, and high reduction efficiency. Subsequently, we employed a two-step melt blending approach to fabricate PP/TrGO nanocomposites with uniform dispersion in the PP matrix. Our findings reveal that under a stress of 25 MPa, the creep failure lifetime of PP incorporating 2.0 wt% TrGO can be improved by 21.5 times compared to neat PP. It is postulated that when TrGO content surpasses 1.0 wt%, an effective particle network structure forms within the PP matrix. This homogeneously dispersed TrGO nanosheets network structure hinders the migration and rearrangement of PP molecular chains, enabling the composite to withstand prolonged stress without experiencing structural failure. By adopting the critical failure strain as a criterion, and coupling it with the time-strain superposition method, we established the generalized curves of creep compliance for PP and its nanocomposites, enabling the prediction of their creep failure lifetimes. The experimental results exhibited strong agreement with the predicted values, successfully predicting the creep failure lifetime for this composite material system. This approach offers a new perspective for developing long-lasting, durable polypropylene materials and products and allows for rapid evaluation of their service lifetimes.

EXPERIMENTAL

Materials

Natural graphite (NG) with a particle size of ≤30 μm and purity of ≥99.85% was obtained from Shanghai National Pharmaceutical Chemical Company. Isotactic polypropylene (*i*PP, T30s) was sourced from Dushanzi Petrochemical Company, which features a melt flow rate (MFR) of 2.9 g/10min, a weight-average molecular weight of 39.9×10^4 g·mol^{-1}, and a ratio of weight-average molecular weight to number-average molecular weight of 4.6. Solvents and reagents used in the experiments, including 98% concentrated sulfuric acid, 36% concentrated hydrochloric acid, potassium permanganate, sodium nitrate, 30% hydrogen peroxide, and tetrahydrofuran, were produced by Chengdu Kelong Chemical Reagent, China.

Preparation of TrGO and PP/TrGO Nanocomposites

Graphene oxide (GO) was prepared using an improved Hummers method,[23] and then thermally reduced graphene oxide (TrGO) was produced through a thermal reduction process.[22] Although previous studies have reported that adding compatibilizers[24] or modifying the graphene surface[11,16,25] can enhance compatibility between non-polar PP and graphene, leading to more uniformly dispersed graphene in polymer matrix, these approaches often introduce complexity to the research system. To enhance the dispersion of TrGO within the PP matrix, we initially prepared a pre-mixture of PP granules coated with TrGO. The process involved adding TrGO to 70 mL of tetrahydrofuran and ultrasonically treating the mixture at 800 W power for 20 min, resulting in pre-exfoliated and dispersed TrGO dispersion. Subsequently, PP powder was incorporated into the dispersion, and the solvent was evaporated at 75 °C. After complete evaporation, the pre-mixture was dried in a 60 °C vacuum oven for 48 h to remove residual solvent, yielding PP/TrGO pre-mixtures containing 0.5 wt%, 1.0 wt% and 2.0 wt% TrGO. Using a torque rheometer (XSS-300), the pre-mixtures were melt-blended for 10 mins to obtain PP/TrGO nanocomposites, designated as PP-0.5, PP-1.0, and PP-2.0. The blending conditions were set at a speed of 50 rpm and a temperature of 180 °C. Neat PP was also obtained using the same preparation method for comparison purposes. Finally, the samples were vacuum-molded into sheets measuring 12 mm × 12 mm × 0.5 mm, which were used for subsequent dynamic mechanical thermal analysis, tensile and creep testing.

Mechanical Properties Tests

We utilized a micro-tensile testing machine (TST 350, Linkam Scientific Instruments, 200 N force sensor, 0.01 N resolution) to conduct uniaxial tensile and creep experiments on the samples. The temperature for both tensile and creep tests was set at 30 °C. Prior to each tensile and creep test, the samples were equilibrated for 15 min at 30 °C to ensure a stable thermal equilibrium state during testing. The tensile specimens were dumbbell-shaped, with a gauge length of 20 mm and a width of 2 mm. The uniaxial tensile tests were carried out at a strain rate of 100 μm/s. For the creep tests, we employed the same stress levels instead of the same yield stress percentages to ensure experimental consistency.[26–28]

Characterization

The dispersion of TrGO in the PP matrix was investigated using scanning electron microscopy (SEM) with an FEI Inspect F50 instrument (USA). The samples analyzed were PP-2.0 composite sheets. To observe the dispersion and exfoliation state of TrGO within the polypropylene matrix, transmission electron microscopy (TEM) was employed. The test samples were cryo-ultrathin sections of the PP-2.0 sheets, and the testing was per-

https://doi.org/10.1007/s10118-023-3028-x

formed using an FEI Tecnai F20 instrument (USA) at room temperature with an acceleration voltage of 20 kV. Rheological tests were conducted using a strain-controlled rheometer (ARES, TA Instruments, USA) fitted with a 25 mm parallel plate. A dynamic frequency sweep mode was used at 1% strain and a temperature of 190 °C. Differential scanning calorimetry (DSC, Q20, TA Instruments, USA) was utilized to characterize the crystallization behavior of the samples. Approximately 5–10 mg of each sample was heated from 30 °C to 200 °C at a rate of 10 °C/min, held at 200 °C for 3 min and subsequently cooled to 80 °C at the same rate. The crystallinity (X_c) of the PP samples was determined using the following Eq. (1):

$$X_c = \frac{\Delta H_m}{\left(F \times \Delta H_m^0\right) \times 100\%} \quad (1)$$

where ΔH_m represents the melting enthalpy of PP, ΔH_m^0 corresponds to the melting enthalpy of fully crystalline PP (206 J/g, referred to Ref. [29]), and F denotes the content of PP in the sample. The crystallinity was calculated using the melting curve, which has a strong correlation with the mechanical properties of the samples. Dynamic mechanical thermal analysis (DMTA, Q800, TA Instruments, USA) in bending mode was employed to analyze the dynamic mechanical properties of PP and its composites. Measurements were taken over a temperature range of −40 °C to 100 °C, with a heating rate of 3 °C/min and a deformation amplitude of 1 mm.

RESULTS AND DISCUSSION

Dispersion of TrGO in PP Matrix

Fig. 1 presents the SEM and TEM images of the nanocomposite material containing 2.0 wt% TrGO. The SEM images reveal that TrGO exhibits some aggregations within the PP matrix, forming small clusters (indicated by yellow arrows). This is attributed to the poor compatibility between TrGO and the non-polar PP matrix.[30] We further investigated the exfoliation and dispersion of TrGO using TEM. As depicted in Fig. 1(b), a majority of the TrGO layers were exfoliated into single or few-layer structures and dispersed in a curled configuration within the PP matrix. Thus, the microscopic characterization results suggest that TrGO is predominantly exfoliated into single layers in the PP matrix, albeit with some aggregation present. Considering the low content of TrGO and the significant correlation between the storage modulus (G') of polymer materials and the dispersion of fillers in the polymer matrix during dynamic frequency sweeps in rheological tests,[31] we conducted rheological tests on the PP/TrGO nanocomposites to further examine the dispersion and exfoliation state of TrGO in PP matrix. Fig. 1(c) displays the variation of G' with angular frequency (ω) for PP and its composites. It is evident that as the TrGO content increases, the G' of the composites also rises. When the TrGO content exceeds 1.0 wt%, an elastic modulus plateau emerges in the low-frequency region, suggesting the formation of an effective TrGO particle network structure in PP matrix. With a further increase in TrGO content, the elastic modulus plateau region becomes more pronounced, indicating enhanced dispersion of TrGO in PP and the formation of a more robust network structure.[32,33] The SEM, TEM and rheological test results demonstrate that despite the presence of small aggregations, most TrGO layers are exfoliated into single or few-layer structures and uniformly dispersed within the PP matrix, forming particle network structures at higher concentrations.

Fig. 2(a) exhibits the enthalpy changes curves during the DSC heating process for neat PP and its nanocomposites. The calculated crystallinities for neat PP, PP-0.5, PP-1.0 and PP-2.0 nanocomposites are 40.7%, 40.9%, 41.5% and 41.4%, respectively. The incorporation of TrGO at higher concentrations results in a minor increase in the crystallinity of the nanocomposites, which is likely due to the heterogeneous nucleation effect triggered by the addition of TrGO, consequently causing a slight increase in the crystallization rate and crystallinity of PP.[34] Additionally, we employed dynamic mechanical property analysis to explore the temperature dependence of the loss factor for PP and its composites, as depicted in Fig. 2(b). The glass transition temperatures (T_g, obtained from the peak values) for neat PP, PP-0.5, PP-1.0 and PP-2.0 composites are 21.5, 21, 20.5 and 20.4 °C, respectively. As the TrGO content increases, the T_g exhibits a slight reduction. This phenomenon may be attributed to the van der Waals forces, which govern both the intermolecular forces among PP molecular chains and the forces between PP molecular chains and TrGO. These forces do not hinder the mobility of PP chain segments. In TrGO aggregation regions, the distance between PP molecular chains expands, resulting in a decrease in intermolecular forces and causing the glass transition temperature to shift towards lower values.[35]

Tensile Creep Behavior of PP/TrGO Nanocomposites

The mechanical property of PP and its nanocomposites at 30 °C were evaluated using uniaxial tensile tests, with the tensile modulus (E_y) and yield stress (σ_s) for each sample presented in Table 1. It can be observed that the incorporation of 0.5 wt% TrGO increases the tensile modulus of PP from 1264 MPa to 1394 MPa. As the TrGO content increases, the tensile modulus of the nanocomposites continues to improve, with the PP-2.0 nanocomposite exhibiting a tensile modulus of 1640 MPa. Simultaneously, the nanocomposites' tensile strength exhibits a minor enhancement. The uniaxial tensile test results indicate that the incorporation of TrGO yields a reinforcing effect. This enhancement can be attributed to the specific surface area effect of the TrGO nanosheets, which facilitates interaction with multiple PP molecular chains, transferring more load and promoting uniform stress distribution throughout the material.[11] Meanwhile, the rigidity of the TrGO nanosheets hinders the slippage and rearrangement of the PP molecular chains, thereby elevating the tensile modulus and yield stress.[36]

Furthermore, we investigated the creep behavior of PP and its nanocomposites at 30 °C under different stress levels as depicted in Fig. 3. Creep experiments were conducted at stress levels below 70% of the composite's yield stress,[3] specifically at 22, 23, 24 and 25 MPa, to study the influence of TrGO on the creep behavior of PP. Typically, the creep behavior of polymer materials comprises four deformation regions: instantaneous deformation, primary creep where the creep rate gradually decreases, secondary creep where the creep rate remains constant, and tertiary creep where the creep rate rapidly increases, leading to creep failure. The critical failure strain, ε_{cr}, is defined as the last point of the constant strain rate in the secondary creep stage, as shown by the dashed line in Fig. 3. The corresponding time for ε_{cr} represents the

https://doi.org/10.1007/s10118-023-3028-x

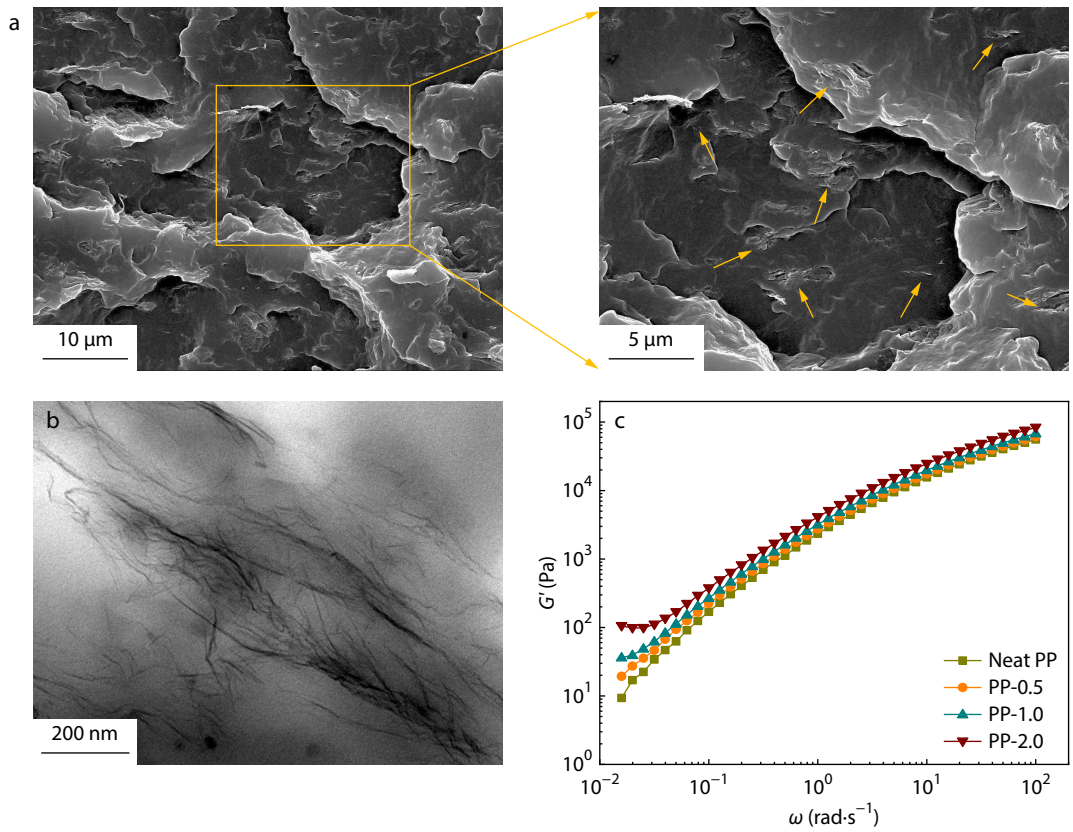

Fig. 1 (a) SEM images of the fractured surfaces of PP/TrGO (2 wt%) nanocomposite; (b) TEM image of the fractured surfaces of PP/TrGO (2 wt%) nanocomposite; (c) Storage modulus (G') as a function of frequency (ω) for neat PP and PP/TrGO nanocomposites filled with different loadings of TrGO at strain of 1% and temperature of 190 °C.

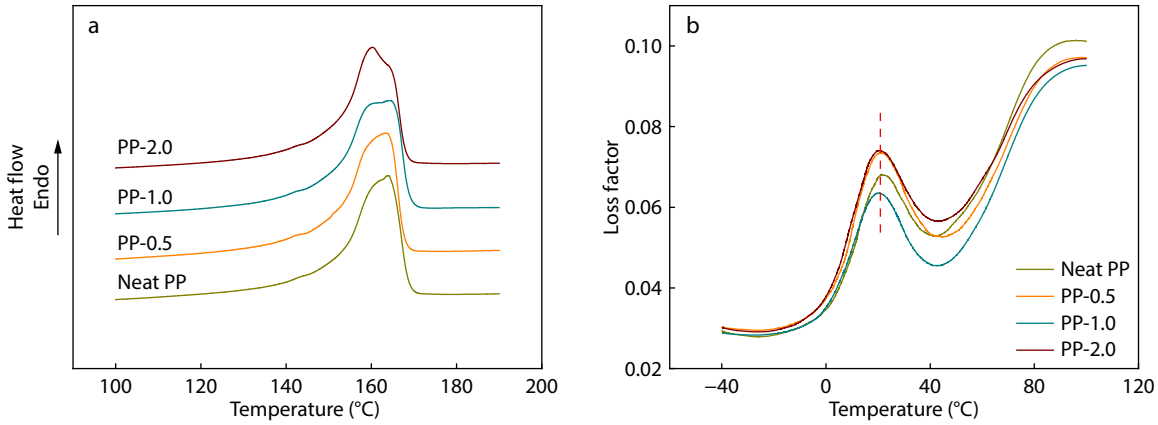

Fig. 2 (a) DSC melting curves for PP and its nanocomposites; (b) Loss factor as a function of temperature for PP and its nanocomposites.

Table 1 The mechanical property of PP and its nanocomposites.

Mechanical property (MPa)	Neat PP	PP-0.5	PP-1.0	PP-2.0
E_y	1264±115	1394±102	1439±62	1640±75
σ_s	30.4±1.8	32.3±2.1	32.7±1.9	32.3±1.9

*E_y is the Young's modulus and σ_s is the yield stress.

creep failure lifetime.[37] The results indicate that, for a given sample, the critical failure strain, ε_{cr}, is independent of the applied stress magnitude, consistent with previous findings.[3,17] Additionally, as the stress increases, the creep rate accelerates rapidly, and the creep failure lifetime significantly decreases.

Fig. 4 illustrates the creep curves of PP and its nanocomposites under identical stress conditions. As depicted in Fig. 4, TrGO primarily reduces the secondary creep rate, with the effect becoming more pronounced as the TrGO content in-

https://doi.org/10.1007/s10118-023-3028-x

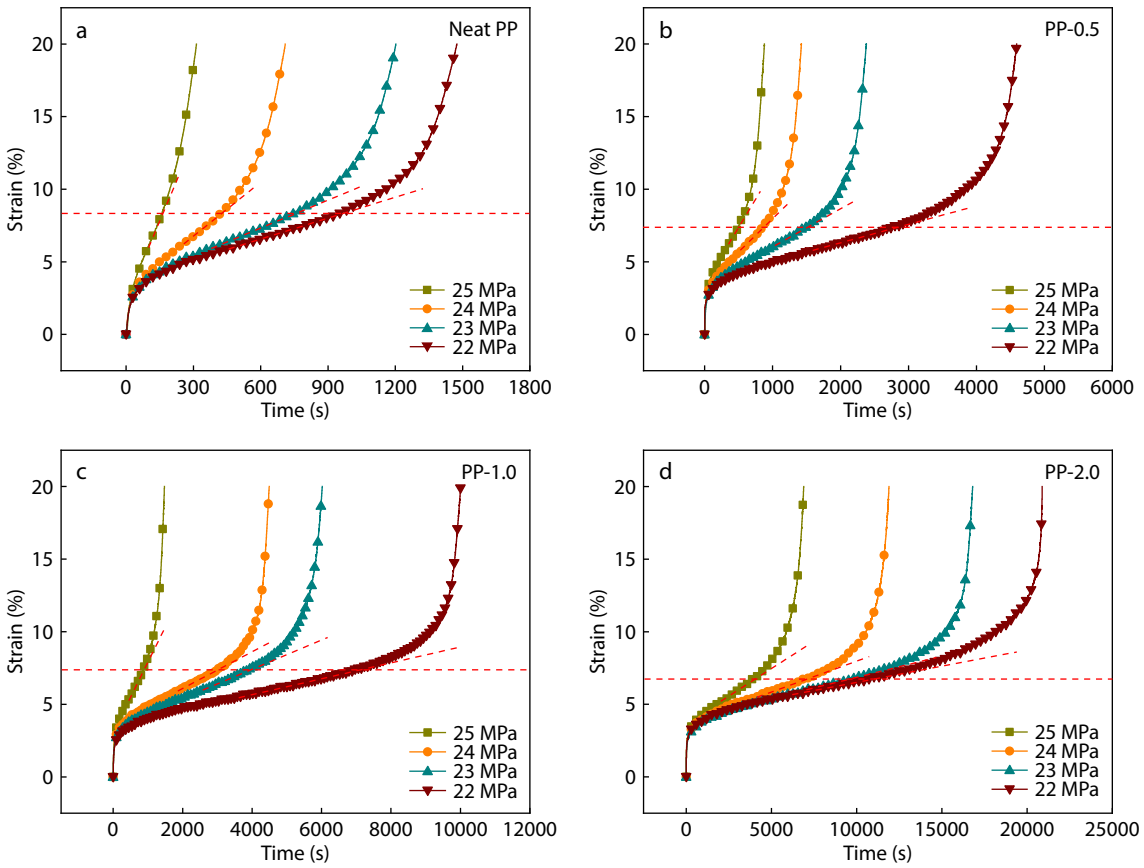

Fig. 3 Tensile creep strain as a function of time under 22, 23, 24 and 25 MPa for neat PP, PP-0.5, PP-1.0 and PP-2.0 nanocomposites.

creases, suggesting that the addition of TrGO notably prolongs the creep deformation time for PP, signifying that the incorporation of TrGO enhances the creep resistance of the PP. One possible explanation for this phenomenon is that the layered structure of TrGO contributes to a more uniform load distribution, thereby minimizing the stress exerted on the molecular chains and consequently decelerating the creep rate of the composite material. Another reason to consider is the slight increase in crystallinity observed in PP/TrGO composites, which aids in restricting the motion of PP molecular chains and further improving the material's creep resistance.[38] Moreover, the inclusion of TrGO decreases the critical failure strain of the composite material, which is probably attributed to TrGO functioning as physical entanglement points. It limits the deformation freedom of PP molecular chains, leading to structural failure when the material experiences larger deformations.

We compared the creep failure lifetime of the PP-2.0 sample with that of neat PP, as presented in Table 2. It is evident that with increasing stress, the creep rates of all samples rise sharply, leading to a significant reduction in creep failure lifetimes. This stress-induced acceleration of creep deformation causes a decrease in the material's creep failure lifetime. The underlying reason is that, under high-stress conditions, the energy barrier for segmental motion of molecular chains diminishes.[39] For PP/TrGO nanocomposites, the incorporation of TrGO notably prolongs the creep failure lifetime of PP. For instance, at a stress of 22 MPa, the creep failure lifetime of the PP-2.0 sample extends to 12232 s, which is 12.8 times longer than that of pristine PP (958 s). This finding suggests that the addition of TrGO substantially enhances the PP's creep failure lifetime. This improvement can be attributed to the restraining effect of TrGO on the mobility of PP molecular chains, rendering the migration and rearrangement of PP molecular chains more challenging. The enhancing effect is more prominent under high-stress conditions; for example, at a stress of 25 MPa, the creep failure lifetime of the PP-2.0 composite is 25.2 times greater than that of pristine PP. This behavior is likely due to the fact that under low-stress levels, molecular chains undergo only local slippage, and their segmental motion capability is partially constrained. In contrast, under high-stress levels, the extension and slippage of molecular chains become more pronounced due to stress activation, resulting in a more evident restriction on the molecular chains. Consequently, the reinforcing effect of TrGO on the PP's creep failure lifetime becomes more significant under high-stress conditions.

According to the creep test results, we found that the incorporation of TrGO remarkably suppresses the creep deformation of PP while enhancing their creep failure lifetime. To gain deeper insights into the mechanism underlying the improvement of PP' creep resistance due to TrGO, we propose a potential reinforcement mechanism as illustrated in Fig. 5. When the PP/TrGO nanocomposite is subjected to stress, the TrGO layers can effectively distribute the load uniformly. This load-sharing capability reduces the stress experienced by the

https://doi.org/10.1007/s10118-023-3028-x

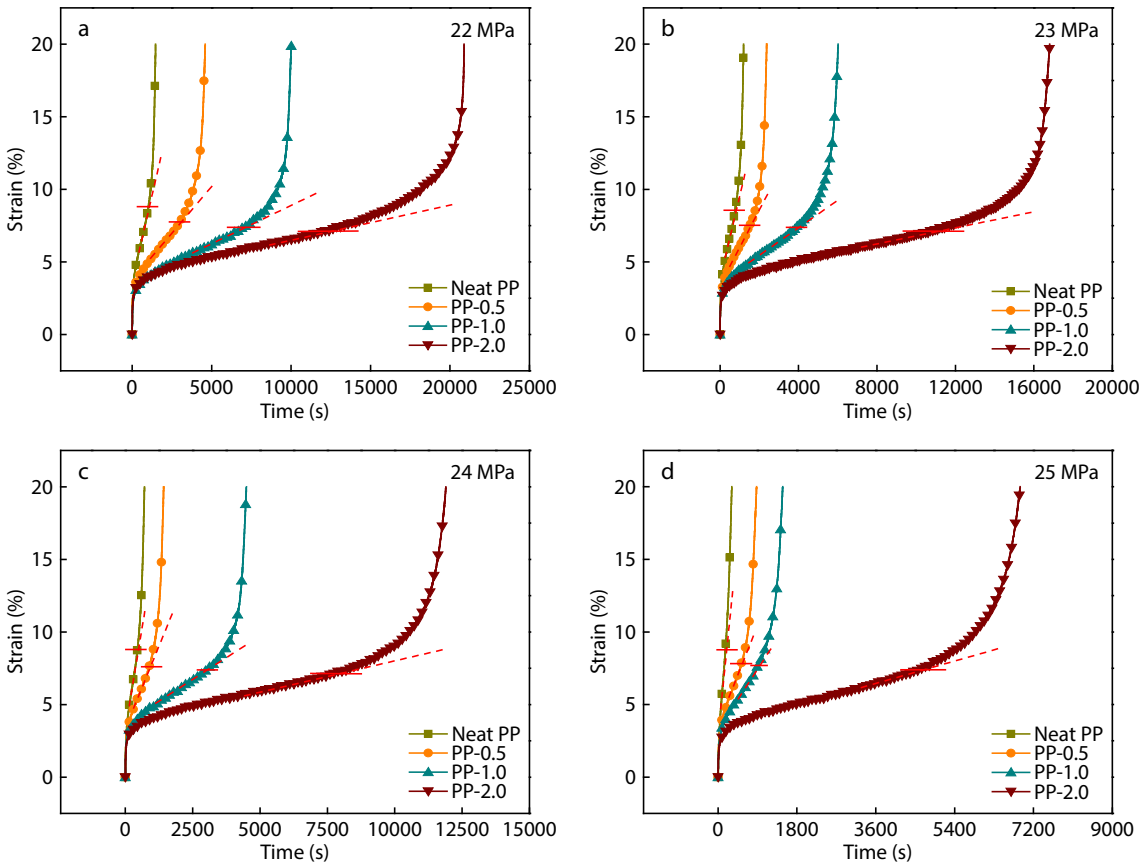

Fig. 4 Creep strain as a function of time for four samples under 22, 23, 24 and 25 MPa. The horizontal bars indicate the transition from secondary creep to tertiary creep.

Table 2 Creep lifetime of four samples under the same stress.

Sress (MPa)	Creep lifetime (s)				
	Neat PP	PP-0.5	PP-1.0	PP-2.0	Ratio
25	165	483	999	4165	25.2
24	433	855	3023	7063	16.3
23	750	1511	3897	9661	12.9
22	958	2795	7178	12232	12.8

molecular chains, subsequently decreasing the rate of molecular chain rearrangement and migration, and ultimately delaying the creep deformation of the material. Furthermore, our rheological tests reveal that when the TrGO content surpasses 1.0 wt%, the TrGO nanosheets form a physical linked particle network structure within the PP matrix. This network structure results in a more pronounced constraining effect on the molecular chains, which in turn leads to a further enhancement of the PP's creep resistance properties. Consequently, the creep failure lifetime of the PP/TrGO nanocomposite material witnesses a significant increase. The presence of this particle network structure plays a crucial role in the observed improvement of the nanocomposite's creep performance. It not only helps to uniformly distribute the applied stress among the molecular chains but also facilitates effective load transfer between the TrGO layers and the PP matrix. This synergistic effect between the TrGO layers and the PP matrix contributes to the remarkable enhancement of the creep resistance and the overall mechanical properties of the nanocomposite material, making it a promising candidate for various applications requiring superior creep resistance and durability.

Prediction of Creep Lifetime of PP/TrGO Nanocomposites

The time-strain superposition method serves as an efficient technique for predicting the time-dependent viscoelastic properties of polymers, polymer blends, and polymer composites under a variety of stress levels.[40] By employing this approach, a generalized compliance curve, characterized by a relatively simple power law, is derived from compliance curves obtained at different stress levels. This allows for the extrapolation of time-dependent creep compliances at lower stresses from the generalized compliance curve, leading to considerable time savings. Although this method has proven effective in describing the time-dependent compliance of materials under multiple stress levels, its application to the lifetime prediction of polymeric ma-

https://doi.org/10.1007/s10118-023-3028-x

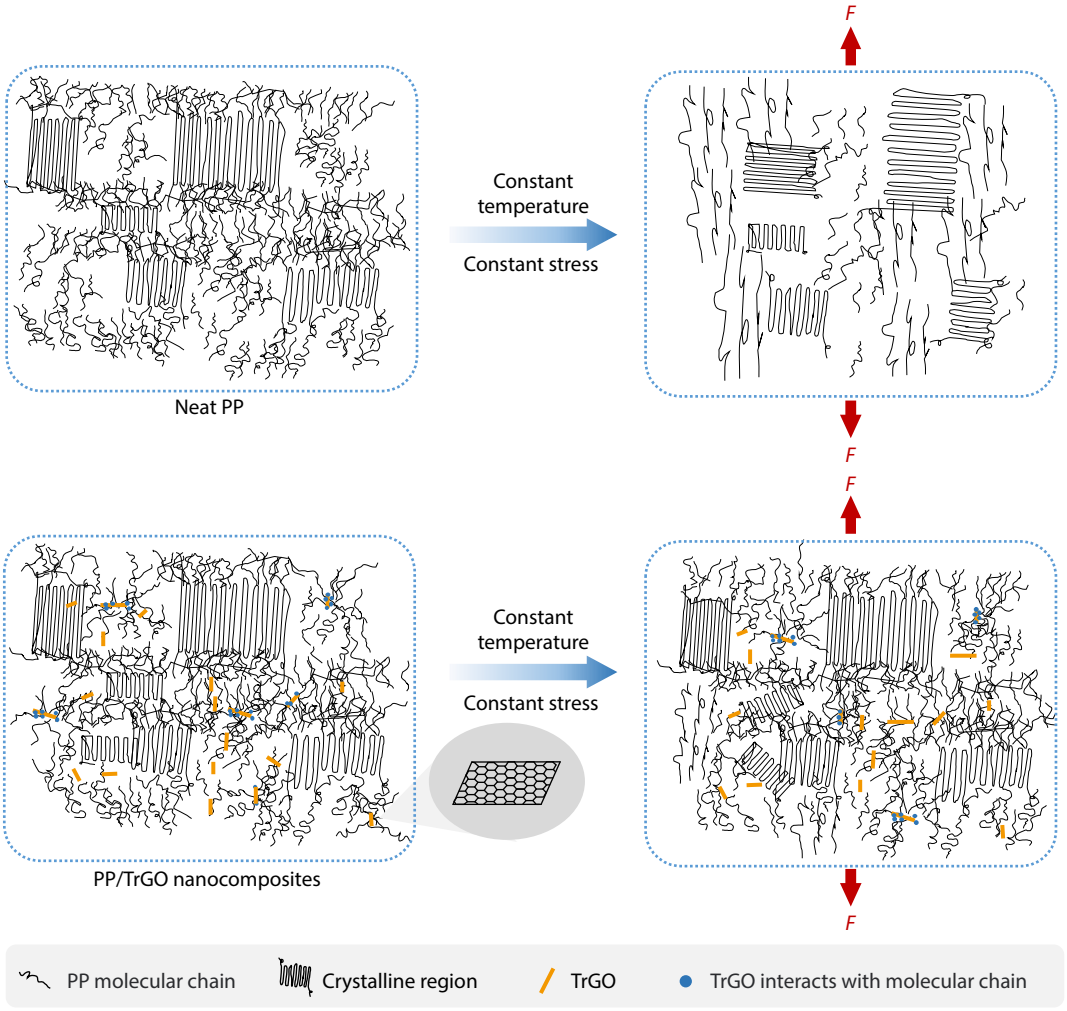

Fig. 5 The possible mechanism on the enhancement of creep lifetimes of PP/TrGO nanocomposites.

terials under creep has been limited due to the absence of a suitable failure criterion. The critical failure strain presents itself as a fitting criterion. Utilizing this criterion, we have successfully predicted the creep failure lifetime of PP/clay nanocomposites under low-stress conditions by analyzing their creep failure lifetime at high-stress conditions.[3] As a result, this model holds promise for predicting the creep failure lifetime of PP/TrGO nanocomposite systems, further expanding its potential applications.

The time-strain superposition method is based on accelerated creep experimental data at higher stress levels, aiming to construct a universal creep compliance master curve to describe the time-dependent viscoelastic behavior of polymer materials. Creep compliance, $D(t)$, is defined as the ratio of strain (ε) to stress level (σ). Fig. 6 illustrates the time-dependent evolution of creep compliance for PP and its composites under various stress levels. As observed, creep compliance consistently increases with higher stress levels, suggesting that PP and its nanocomposites demonstrate typical nonlinear viscoelastic behavior within the investigated stress range.

The creep behavior of materials can be described by the power law, as follows:

$$\log D(t^*, \sigma) = \log C^*(\sigma) + n^* \log(t^*) \quad (2)$$

where C^* and n^* are parameters related to t^*, and t^* is the internal time used to describe the instantaneous delay rate change conversion. When materials are subjected to stress, the increase in strain can cause changes in the free volume, resulting in the stretched creep exhibiting nonlinear characteristics.[41] Therefore, unlike the real time t, t^* represents the internal time in the hypothetical reference state. The acceleration factor $\log a_\varepsilon(t)$ between the internal time t^* and the real time t can be calculated using the following equation:[3]

$$\log t^* = \log t - \log a_\varepsilon(t) = \log t + (B/2.303)\frac{[(1-2\nu)M\varepsilon(t)/(f_g + a_T(T - T_g))]}{[(1-2\nu)M\varepsilon(t) + (f_g + a_T(T - T_g))]} \quad (3)$$

where B is a material constant, typically assigned a value of 1; ν is the Poisson's ratio, with a value of 0.4; M is the strain amplification factor, defined as the ratio of real strain (microscopic strain) to measured strain (macroscopic strain), and is related to the crystallinity of the composite material. Based on the crystallinity values obtained from DSC tests of PP and its composites, the calculated M values for PP, PP-0.5, PP-1.0, and PP-2.0 samples are 1.5, 1.5, 1.51, and 1.51, respectively; f_g is the free volume fraction in the reference state, with a value of 0.025; T is the temper-

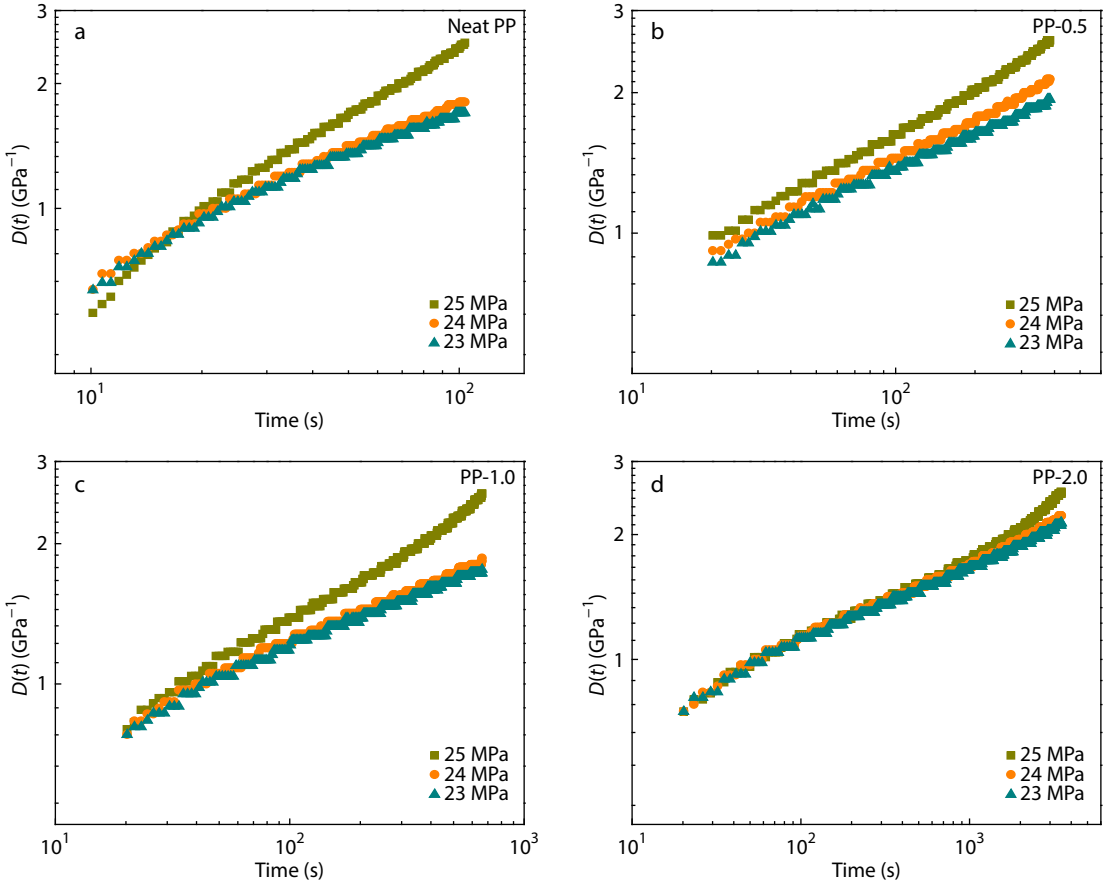

Fig. 6 Creep compliance as a function of time under the stresses of 23, 24 and 25 MPa for PP and it nanocomposites.

ature (absolute temperature, K) used for the creep experiment; α_T is the thermal expansion coefficient (K^{-1}), with a value of $3.3\times10^{-4}K^{-1}$; T_g is the glass transition temperature of the material, obtained from DMA testing; and $\varepsilon(t)$ is the time-dependent strain.

After applying the time acceleration factor conversion, we obtained the double logarithmic generalized curves for creep compliance and internal time of the PP and its nanocomposites under stress of 23, 24 and 25 MPa, as illustrated in Fig. 7. When plotting the creep curves as logarithmic graphs with respect to the internal conversion time t^*, the creep compliance curves for PP and its nanocomposites under various stress levels align on a single line. This observation signifies the effectiveness of the time-strain superposition model in characterizing the creep behavior of PP and its nanocomposites. By performing linear regression on the compliance generalized curves of the materials under different stress levels, we derived the generalized curve parameters C^* and n^*, with the corresponding data presented in Table 3. The C^* and n^* values, obtained from linear regression, exhibit minimal sensitivity to stress and display only minor fluctuations, which confirms the satisfactory superposition effect of the model. Subsequently, we calculated the average values of C^* and n^* under different stress conditions to establish the power law equation for creep compliance and internal conversion time. This equation served as the foundation for predicting the creep failure lifetimes of various polymer materials under low-stress conditions.

Based on the creep tests, we determined the critical failure strain for PP and its nanocomposites. Dividing the critical failure strain by the corresponding applied stress yielded the critical failure compliance (D_{crit}) under different stress conditions. For neat PP, PP-0.5, PP-1.0 and PP-2.0 composites subjected to a 22 MPa stress, the calculated D_{crit} values were 3.773, 3.364, 3.318 and 3.091, respectively. Combining the aforementioned relationship between creep compliance and internal conversion time t^*, we calculated the internal conversion time at the critical failure compliance. Subsequently, we determined the required time for critical failure to occur by applying the relationship between real time t and internal conversion time t^*, as presented in Eq. (3), which enabled the prediction of the materials' creep failure lifetimes. Employing the critical failure compliance as the criterion, we predicted the creep lifetimes of PP and its composites under various stress conditions using the established time-strain superposition model. The comparison between the predicted and experimental values is depicted in Fig. 8, which demonstrates a reasonably good agreement between the predicted creep failure lifetimes and experimental values. The experimental creep failure lifetimes of PP-0.5, PP-1.0, and PP-2.0 composites under a stress of 22 MPa were 2609, 7957 and 16285 s, respectively, while the predicted values were 2795, 7178 and 12232 s. With the maximum deviation of approximately 30%, the results indicate that we can predict the creep failure life-

https://doi.org/10.1007/s10118-023-3028-x

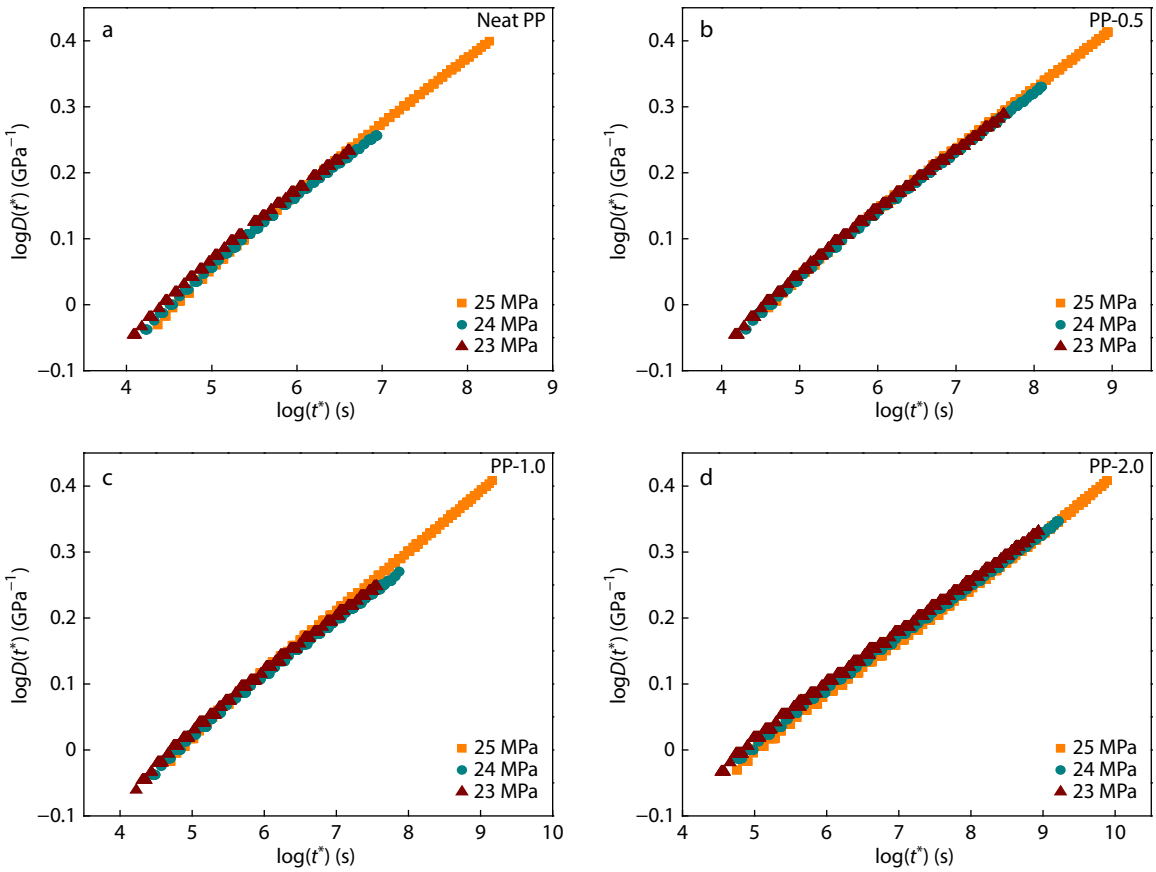

Fig. 7 The generalized curves of creep compliance as a function of internal time under the stresses of 23, 24 and 25 MPa for PP and its nanocomposites.

Table 3 Values of the parameters of C^* and n^* fitted from the generalized curves.

Specimen	Stress (MPa)	log(C^*)	n^*	R^2
Neat PP	25	−0.4449	0.1025	0.9995
	24	−0.4345	0.0998	0.9992
	23	−0.4214	0.0991	0.9985
Average	–	−0.4336	0.1005	–
PP-0.5	25	−0.3977	0.0906	0.9999
	24	−0.3956	0.0896	0.9994
	23	−0.3787	0.0875	0.9985
Average	–	−0.3907	0.0892	–
PP-1.0	25	−0.4234	0.0905	0.9998
	24	−0.3792	0.0822	0.9988
	23	−0.3743	0.0823	0.998
Average	–	−0.3923	0.085	–
PP-2.0	25	−0.41888	0.0831	0.9992
	24	−0.38161	0.0799	0.9994
	23	−0.371	0.0804	0.9992
Average	–	−0.3903	0.0811	–

times of PP/TrGO nanocomposites under low-stress conditions through high-stress creep failure tests, saving significant testing time for the rapid assessment of their lifetimes in real service conditions.

CONCLUSIONS

Through SEM, TEM and rheological characterization tests, it was demonstrated that effective particles network structures formed within the PP matrix when the TrGO content exceeded 1.0 wt%. This led to a significant enhancement in the creep resistance of PP/TrGO nanocomposites. For instance, the creep failure lifetime of PP-2.0 composites under a 25 MPa stress increased by 21.5 times compared to neat PP. This improvement can be attributed to the TrGO layers acting as physical linking points, which evenly distribute the load and restrict the migration and rearrangement of molecular chains, thus enabling the material to withstand prolonged stress without structural failure. By em-

https://doi.org/10.1007/s10118-023-3028-x

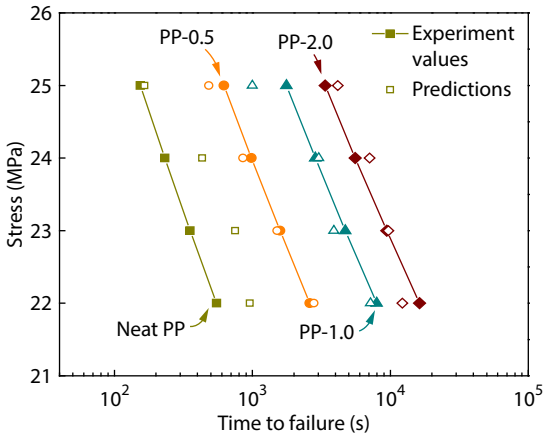

Fig. 8 The theoretical and experimental creep failure lifetime for PP and its nanocomposites. Open symbols denote observations and Solid symbols represent the predictions. The solid lines are used to guide the eyes.

ploying the critical failure strain as a criterion and utilizing the time-strain superposition method, the generalized curves of creep compliance for PP and its nanocomposites was established. This allowed for the prediction of their creep failure lifetimes, with the experimental and predicted values showing minimal fluctuations. The results confirm the applicability of this predictive model to the PP/TrGO nanocomposite system, emphasizing the significance of the findings for understanding the creep behavior of these materials and facilitating the evaluation of their service life. Furthermore, these findings show the potential to impact various industries, including automotive, aerospace and construction, where materials with enhanced creep resistance are highly desirable. By understanding the impact of TrGO content on the creep performance of PP composites, it is possible to optimize material selection and processing, ultimately leading to the development of more durable and efficient materials for various applications.

Conflict of Interests

The authors declare no interest conflict.

ACKNOWLEDGMENTS

This work was financially supported by Natural Science Foundation of Sichuan Province (No. 2022NSFSC0296), the National Natural Science Foundation of China (Nos. 51903118 and U19A2096), and State Key Laboratory of Polymer Materials Engineering (No. sklpme2020-1-07, Sichuan University).

REFERENCES

1 Maubane, L.; Lekalakala, R.; Orasugh, J. T.; Letwaba, J. Effect of short-chain architecture on the resulting thermal properties of polypropylene. *Polymer* **2023**, *264*, 125533.
2 Khoury Moussa, H.; Challita, G.; Badreddine, H.; Montay, G.; Guelorget, B.; Vallon, T.; Yared, W.; Abi Rizk, M.; Alhussein, A. Enhancement of mechanical properties of high modulus polypropylene grade for multilayer sewage pipes applications. *J. Appl. Polym. Sci.* **2022**, *140*, e53314.
3 Lv, Y.; Huang, Y.; Kong, M.; Yang, J.; Yang, Q.; Li, G. Creep lifetime prediction of polypropylene/clay nanocomposites based on a critical failure strain criterion. *Compos. Sci. Technol.* **2014**, *96*, 71–79.
4 Novoselov, K. S.; Geim, A. K.; Morozov, S. V.; Jiang, D.; Zhang, Y.; Dubonos, S. V.; Grigorieva, I. V.; Firsov A. A.. Electric field effect in atomically thin carbon films. *Science* **2004**, *306*, 666–669.
5 Geim, A. K.; Novoselov, K. S. The rise of graphene. *Nat. Mater.* **2007**, *6*, 183–191.
6 Bustillos, J.; Montero, D.; Nautiyal, P.; Loganathan, A.; Boesl, B.; Agarwal, A. Integration of graphene in poly(lactic) acid by 3D printing to develop creep and wear-resistant hierarchical nanocomposites. *Polym. Compos.* **2018**, *39*, 3877–3888.
7 Talukder, N.; Wang, Y.; Nunna, B. B.; Lee, E. S. Nitrogen-doped graphene nanomaterials for electrochemical catalysis/reactions: a review on chemical structures and stability. *Carbon* **2021**, *185*, 198–214.
8 Bhardwaj, S. K.; Mujawar, M.; Mishra, Y. K.; Hickman, N.; Chavali, M.; Kaushik, A. Bio-inspired graphene-based nano-systems for biomedical applications. *Nanotechnology* **2021**, *32*, 502001
9 Hone, C. L. X. W. J. W. K. J. Measurement of the elastic properties and intrinsic strength of monolayer graphene. *Science* **2008**, *321*, 385–388.
10 Kalaitzidou, K.; Fukushima, H.; Drzal, L. T. Mechanical properties and morphological characterization of exfoliated graphite-polypropylene nanocomposites. *Compos. Part A* **2007**, *38*, 1675–1682.
11 Yun, Y. S.; Bae, Y. H.; Kim, D. H.; Lee, J. Y.; Chin, I. J.; Jin, H. J. Reinforcing effects of adding alkylated graphene oxide to polypropylene. *Carbon* **2011**, *49*, 3553–3559.
12 El Achaby, M.; Arrakhiz, F. E.; Vaudreuil, S.; el Kacem Qaiss, A.; Bousmina, M.; Fassi-Fehri, O. Mechanical, thermal, and rheological properties of graphene-based polypropylene nanocomposites prepared by melt mixing. *Polym. Compos.* **2012**, *33*, 733–744.
13 Zandiatashbar, A.; Picu, C. R.; Koratkar, N. Control of epoxy creep using graphene. *Small.* **2012**, *8*, 1676–1682.
14 Tang, L. C.; Wang, X.; Gong, L. X.; Peng, K.; Zhao, L.; Chen, Q.; Wu, L. B.; Jiang, J. X.; Lai, G. Q. Creep and recovery of polystyrene composites filled with graphene additives. *Compos. Sci. Technol.* **2014**, *91*, 63–70.
15 Wang, X.; Gong, L. X.; Tang, L. C.; Peng, K.; Pei, Y. B.; Zhao, L.; Wu, L. B.; Jiang, J. X. Temperature dependence of creep and recovery behaviors of polymer composites filled with chemically reduced graphene oxide. *Compos. Part A* **2015**, *69*, 288–298.
16 Naz, A.; Riaz, I.; Jalil, R.; Afzal, S.; Qayyum khan, A. Creep strain and recovery analysis of polypropylene composites filled with graphene nano filler. *Polymer* **2021**, *217*, 123423.
17 Liu, X.; Huang, Y.; Deng, C.; Wang, X.; Tong, W.; Liu, Y.; Huang, J.; Yang, Q.; Liao, X.; Li, G. Study on the creep behavior of polypropylene. *Polym. Eng. Sci.* **2009**, *49*, 1375–1382.
18 Hiss, R.; Hobeika, S.; Lynn, C.; Strobl, G. Network stretching, slip processes, and fragmentation of crystallites during uniaxial drawing of polyethylene and related copolymers. A comparative study. *Macromolecules* **1999**, *32*, 4390–4403.
19 Kolařík, J. Tensile creep of thermoplastics: time-strain superposition of non-iso free-volume data. *J. Polym. Sci., Part B: Polym. Phys.* **2003**, *41*, 736–748.
20 Kolařiak, J.; Fambri, L.; Pegoretti, A.; Penati, A.; Goberti, P. Prediction of the creep of heterogeneous polymer blends: rubber-toughened polypropylene/poly(styrene-co-acrylonitrile). *Polym. Eng. Sci.* **2002**, *42*, 161–169.
21 Dorigato, A.; Pegoretti, A.; Kolařík, J. Nonlinear tensile creep of linear low density polyethylene/fumed silica nanocomposites:

time-strain superposition and creep prediction. *Polym. Compos.* **2010**, *31*, 1947–1955.
22 McAllister, M. J.; Li, J.-L.; Adamson, D. H.; Schniepp, H. C.; Abdala, A. A.; Liu, J.; Herrera-Alonso, M.; Milius, D. L.; Car, R.; Prud'homme, R. K. Single sheet functionalized graphene by oxidation and thermal expansion of graphite. *Chem. Mater.* **2007**, *19*, 4396–4404.
23 Hummers Jr, W. S.; Offeman, R. E. Preparation of graphitic oxide. *J. Am. Chem. Soc.* **1958**, *80*, 1339–1339.
24 Loh, K. P.; Bao, Q.; Ang, P. K.; Yang, J. The chemistry of graphene. *J. Mater. Chem.* **2010**, *20*, 2277–2289.
25 Hsiao, M. C.; Liao, S. H.; Lin, Y. F.; Wang, C. A.; Pu, N. W.; Tsai, H. M.; Ma, C. C. M. Preparation and characterization of polypropylene-graft-thermally reduced graphite oxide with an improved compatibility with polypropylene-based nanocomposite. *Nanoscale* **2011**, *3*, 1516–1522.
26 Yang, J.-L.; Zhang, Z.; Schlarb, A. K.; Friedrich, K. On the characterization of tensile creep resistance of polyamide 66 nanocomposites. Part II: modeling and prediction of long-term performance. *Polymer* **2006**, *47*, 6745–6758.
27 Ganss, M.; Satapathy, B. K.; Thunga, M.; Weidisch, R.; Pötschke, P.; Janke, A. Temperature dependence of creep behavior of PP-MWNT nanocomposites. *Macromol. Rapid Commun.* **2007**, *28*, 1624–1633.
28 Varela-Rizo, H.; Weisenberger, M.; Bortz, D.; Martin-Gullon, I. Fracture toughness and creep performance of PMMA composites containing micro and nanosized carbon filaments. *Compos. Sci. Technol.* **2010**, *70*, 1189–1195.
29 Jia, Y.; Peng, K.; Gong, X. l.; Zhang, Z. Creep and recovery of polypropylene/carbon nanotube composites. *Int. J. Plast.* **2011**, *27*, 1239–1251.
30 Lv, C.; Xue, Q.; Xia, D.; Ma, M.; Xie, J.; Chen, H. Effect of chemisorption on the interfacial bonding characteristics of graphene-polymer composites. *J. Phys. Chem. C.* **2010**, *114*, 6588–6594.
31 Vermant, J.; Ceccia, S.; Dolgovskij, M.; Maffettone, P.; Macosko, C. Quantifying dispersion of layered nanocomposites *via* melt rheology. *J. Rheol.* **2007**, *51*, 429–450.
32 Cassagnau, P. Melt rheology of organoclay and fumed silica nanocomposites. *Polymer* **2008**, *49*, 2183–2196.
33 Lertwimolnun, W.; Vergnes, B. Influence of compatibilizer and processing conditions on the dispersion of nanoclay in a polypropylene matrix. *Polymer* **2005**, *46*, 3462–3471.
34 Xu, J.-Z.; Chen, C.; Wang, Y.; Tang, H.; Li, Z. M.; Hsiao, B. S. Graphene nanosheets and shear flow induced crystallization in isotactic polypropylene nanocomposites. *Macromolecules* **2011**, *44*, 2808–2818.
35 Aliotta, L.; Gigante, V.; Molinari, G.; D'Ambrosio, R.; Botta, L.; La Mantia, F. P.; Lazzeri, A. Effect of biobased plasticizers, used as dispersing aids, on mechanical, rheological and thermal properties of micro fibrillated cellulose (MFC)/poly(lactic acid) (PLA) biocomposites over the time: how MFC controls the plasticizer migration? *Cellulose* **2022**, *30*, 2237–2252.
36 Yaragalla, S.; Zahid, M.; Panda, J. K.; Tsagarakis, N.; Cingolani, R.; Athanassiou, A. Comprehensive enhancement in thermomechanical performance of melt-extruded PEEK filaments by graphene incorporation. *Polymers* **2021**, *13*, 1425–1443.
37 Drozdov, A. Creep rupture and viscoelastoplasticity of polypropylene. *Eng. Fract. Mech.* **2010**, *77*, 2277–2293.
38 Ranade, A.; Nayak, K.; Fairbrother, D.; D'Souza, N. A. Maleated and non-maleated polyethylene–montmorillonite layered silicate blown films: creep, dispersion and crystallinity. *Polymer* **2005**, *46*, 7323–7333.
39 Eyring, H. Viscosity, plasticity, and diffusion as examples of absolute reaction rates. *J. Chem. Phys.* **1936**, *4*, 283–291.
40 Kolařík, J.; Pegoretti, A. Non-linear tensile creep of polypropylene: time-strain superposition and creep prediction. *Polymer* **2006**, *47*, 346–356.
41 Jazouli, S.; Luo, W.; Brémand, F.; Vu-Khanh, T. Nonlinear creep behavior of viscoelastic polycarbonate. *J. Mater. Sci.* **2006**, *41*, 531–536.

https://doi.org/10.1007/s10118-023-3028-x